Published in final edited form as:

Cell Rep. 2018 June 05; 23(10): 2915–2927. doi:10.1016/j.celrep.2018.05.024.

Mammalian Auditory Hair Cell Bundle Stiffness Affects Frequency Tuning by Increasing Coupling along the Length of the Cochlea

James B. Dewey[1], **Anping Xia**[2], **Ulrich Müller**[3], **Inna A. Belyantseva**[4], **Brian E. Applegate**[5], and **John S. Oghalai**[1,6,*]

[1]The Caruso Department of Otolaryngology – Head & Neck Surgery, University of Southern California, Los Angeles, CA 90033, USA

[2]Department of Otolaryngology – Head & Neck Surgery, Stanford University, Stanford, CA 94305, USA

[3]The Solomon H. Snyder Department of Neuroscience, School of Medicine, Johns Hopkins University, Baltimore, MD 21205, USA

[4]Laboratory of Molecular Genetics, NIDCD, NIH, Bethesda, MD 20892, USA

[5]Department of Biomedical Engineering, Texas A&M University, College Station, TX 77843, USA

[6]Lead Contact

SUMMARY

The stereociliary bundles of cochlear hair cells convert mechanical vibrations into the electrical signals required for auditory sensation. While the stiffness of the bundles strongly influences mechanotransduction, its influence on the vibratory response of the cochlear partition is unclear. To assess this, we measured cochlear vibrations in mutant mice with reduced bundle stiffness or with a tectorial membrane (TM) that is detached from the sensory epithelium. We found that reducing bundle stiffness decreased the high-frequency extent and sharpened the tuning of vibratory responses obtained postmortem. Detaching the TM further reduced the high-frequency extent of the vibrations but also lowered the partition's resonant frequency. Together, these results demonstrate that the bundle's stiffness and attachment to the TM contribute to passive longitudinal coupling in the cochlea. We conclude that the stereociliary bundles and TM interact to facilitate passive wave propagation to more apical locations, possibly enhancing active wave amplification *in vivo*.

*Correspondence: john.oghalai@med.usc.edu.

AUTHOR CONTRIBUTIONS

J.B.D., B.E.A., and J.S.O. conceived the project and wrote the manuscript. J.B.D. performed vibratory experiments and analyzed data. A.X. performed dissections and imaging of whole-mount preparations. U.M. and I.A.B. provided mouse strains and aided in conceiving the project and interpreting the data. All authors edited the manuscript.

DECLARATION OF INTERESTS

U.M. is a cofounder of Decibel Therapeutics. The other authors declare no competing interests.

SUPPLEMENTAL INFORMATION

Supplemental Information includes one table and can be found with this article online at https://doi.org/10.1016/j.celrep.2018.05.024.

In Brief

The mechanical properties of the cochlear partition determine its vibratory response to sound. Dewey et al. demonstrate that the outer hair cell stereociliary bundles' stiffness and attachment to the tectorial membrane influence the partition's passive vibratory response. The stereociliary bundles facilitate the propagation of cochlear waves to more apical regions.

Graphical Abstract

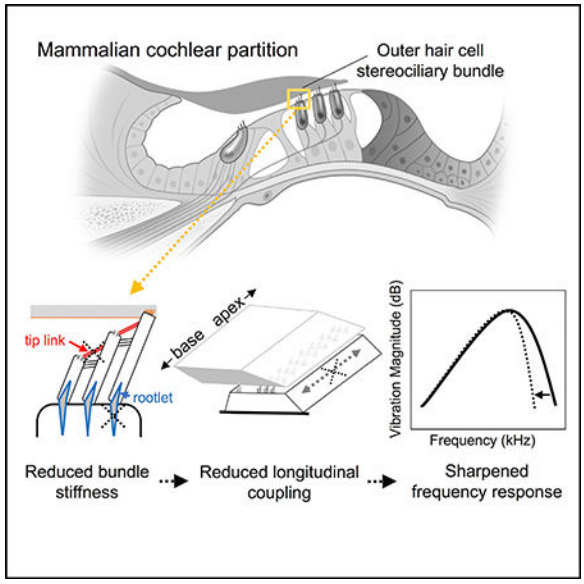

INTRODUCTION

Acoustic stimulation of the mammalian inner ear produces displacement waves on the basilar membrane (BM) that travel from the base of the cochlear spiral toward its apical end. These motions vibrate the organ of Corti and overlying tectorial membrane (TM), thus deflecting the stereociliary bundles of the inner and outer hair cells (IHCs and OHCs, respectively). IHCs provide the primary afferent response of the cochlea. Their bundles are freestanding (Lim, 1986) and stimulated by fluid interactions in the space between the TM and the top surface of the organ of Corti, the reticular lamina (RL) (Guinan, 2012). The mechanical properties of the IHC bundles are therefore thought to have a negligible impact on the vibration of the cochlear partition (Strelioff et al., 1985). In contrast, OHC bundles are firmly attached to the underside of the TM via their tallest stereociliary row and are stimulated by the shearing motion between the RL and TM. OHCs produce forces that increase vibratory magnitudes by more than 1,000-fold (Oghalai, 2004; Robles and Ruggero, 2001). These forces are thought to be dominated by the voltage-dependent electromotile response of the OHC soma (somatic motility) (Brownell et al., 1985; Dallos et al., 2008; Liberman et al., 2002) but may also include contributions from the bundle itself (bundle motility) (Hudspeth, 2014; Kennedy et al., 2005) (Figure 1A).

The stiffness of the OHC bundle is an important property because it affects mechanotransduction and, thus, cochlear amplification. In addition, OHC bundle stiffness

may contribute to the passive mechanical properties of the cochlear partition. However, the stiffness of the bundle relative to the stiffness of the surrounding structures is disputed. While an *in vitro* study of the gerbil cochlea found that the bundles contribute ~25% of the total stiffness of the cochlear partition (Chan and Hudspeth, 2005), comparisons of OHC bundle stiffness measured *in vitro* with the stiffness of the TM measured *in vitro* or *in vivo* have reached varying conclusions. The OHC bundles have been suggested to be much stiffer (Zwislocki and Cefaratti, 1989), similarly stiff (Richter et al., 2007; Shoelson et al., 2004), or much less stiff than the TM (Abnet and Freeman, 2000; Gu et al., 2008). Since the mechanical properties of the BM, organ of Corti, and TM interact to define the vibratory frequency response at a given cochlear location (Figure 1B) (Geisler, 1998; Neely, 1993), these conflicting data indicate that we do not understand how OHC bundles influence the traveling wave.

Here, we measured the frequency response of the cochlear partition noninvasively using volumetric optical coherence tomography and vibrometry (VOCTV) in adult mice with mutations affecting the stiffness of the bundle—due to the absence of the stereociliary tip links or rootlets—and its attachment to the TM. In these mouse models, mechanotransduction and OHC-mediated amplification are impaired, allowing us to study the bundle's contribution to the passive mechanics of the partition. Specifically, we examined how bundle stiffness contributes to the transverse stiffness of the partition, which is critical for defining the frequency at which a given location is tuned. Reducing transverse stiffness would lower the best frequency (BF)—the frequency of maximal vibratory magnitude—and broaden the response bandwidth (Figure 1C). In addition, we studied how the bundles contribute to longitudinal coupling, which theoretically influences the spread of excitation along the cochlear length. Though the radial fibers of the BM suggest that the partition can largely be treated as a series of independent transverse segments (Olson et al., 2012), the BM, organ of Corti, and TM all exhibit some degree of longitudinal coupling (Abnet and Freeman, 2000; von Békésy, 1960; Naidu and Mountain, 2001). This coupling may be a small but, nevertheless, mechanistically important feature of the partition's material properties. Reduced longitudinal coupling is predicted to sharpen the bandwidth of the response at a given location and steepen the slope of the phase versus frequency curve (Figure 1D) (Allen and Sondhi, 1979; Eze and Olson, 2011; Meaud and Grosh, 2010; Wickesberg and Geisler, 1986). Interestingly, our data indicate that the OHC bundles contribute minimally to transverse partition stiffness but substantially to longitudinal coupling.

RESULTS

Vibrations in Wild-Type Mice

We used VOCTV to obtain cross-sectional images of the intact mouse cochlea (Figures 2A and 2E) and measure sound-evoked vibrations from the BM, RL, and TM in the apical turn. Vibrations were measured with the mouse's head rotated so that the BM was tilted counterclockwise by ~60° (average = 63.74 ± 0.80° in 10 mice) relative to a horizontal position (Figure 2E), rather than with the BM perpendicular to the optical path of our system (Figure 2A). In the former orientation, the motions in line with the optical axis can be

considered “semi-radial” as they capture ~87% of the radial and ~50% of the transverse (up-and-down) motion vectors. The total measured motion is the vector sum of components projected from the transverse and radial motions. Measurement of the semi-radial motion was advantageous in that it allowed us to differentiate measurement points on the BM, RL, and TM based on the phase of their vibratory response to intense low-frequency tones.

To illustrate this, the displacement magnitude and phase in response to a 5 kHz, 80 dB sound pressure level (SPL) tone are shown in pseudocolor for each point in a cross-sectional image of a live, wild-type (WT) mouse cochlea when either the transverse (Figures 2B and 2C) or semi-radial (Figures 2F and 2G) motions were measured. In the transverse orientation, phase differences between the BM, RL, and TM were subtle, and the structures largely moved up and down together (Figure 2C). However, in the semi-radial orientation, the RL moved out of phase with the BM and TM (Figure 2G). This anti-phasic motion occurs because the upward motion of the BM translates into an inward pivoting of the RL (Hu et al., 1999; Lee et al., 2016). With the head sufficiently tilted, the motion component projected from the RL’s radial movement was larger than that of its transverse movement and, thus, dominated the motion of the RL in line with the optical axis (Figures 2D and 2H). In live WT mice, this anti-phasic motion was observed most clearly at low- to mid-frequencies (~2–5 kHz) and high stimulus intensities, while it was apparent under all stimulus conditions in dead WT mice and in mutant mice that lacked cochlear amplification. This motion pattern is therefore attributable to passive cochlear mechanics. Note that since the BM moves primarily in the transverse direction (Lee et al., 2016), the BM motion measured in this semi-radial orientation still permits assessment of the transverse partition stiffness. Moreover, since this stiffness largely determines the partition’s BF at a given location, it will influence the partition’s overall frequency response (including the responses of the TM and RL), regardless of measurement angle.

Semi-radial vibrations of the BM, RL, and TM in live WT mice resembled the transverse vibrations of these structures reported previously (Lee et al., 2015, 2016) and exhibited the hallmarks of nonlinear OHC-mediated amplification. This nonlinear amplification is best appreciated by dividing the displacements of the cochlear structures by those of the middle ear to derive the cochlear gain (Figures 3A–3D). In live WT mice, the gain was strongly dependent on both stimulus frequency and level, with the highest gain provided for low-intensity stimuli near 10 kHz, the characteristic frequency (CF) of the measurement location (here, CF refers to the frequency of maximal gain at low stimulus levels in live mice, whereas BF refers more generally to the frequency of maximum response at any given stimulus level). With increasing stimulus level, there was progressively less gain near the CF, the peak gain shifted to lower frequencies, and the response bandwidth broadened. At frequencies much lower than the CF, the gain was less dependent on stimulus level, though level-dependent gain was observed for the RL even at the lowest frequencies, as described previously (Lee et al., 2016; Ren et al., 2016). Vibratory phases (Figures 3E–3H) showed increasing lags as a function of frequency consistent with traveling wave propagation, with a level dependence that was most obvious for the TM (Figure 3G).

Our mutant mouse models all had impaired mechanotransduction by adulthood, so that OHC-mediated amplification was absent (Kitajiri et al., 2010; Schwander et al., 2009; Xia et

al., 2010). Therefore, we focused our comparisons on measurements made after death, which eliminated the confounding effects of amplification in WT mice (Figures 3D and 3I–3L). This allowed us to assess the influence of the stereociliary bundles on the passive mechanics of the cochlea. The loss of amplification postmortem is due to the rapid decline of the metabolically dependent endocochlear potential (Konishi et al., 1961; Russell and Cowley, 1983; Sadanaga and Morimitsu, 1995), which provides the driving force for mechanotransduction currents. While previous reports (e.g., Eze and Olson, 2011) have approximated a passive cochlear condition in live animals by using high stimulus levels, our measurements suggest that this is not adequate in the apex of the mouse cochlea, since death reduced gain at frequencies near the CF for all stimulus levels. However, postmortem response phases were similar to those of responses to high-intensity stimuli in live mice (Figures 3H and 3M–3P). We obtained postmortem measurements from all mice 10–60 min after death, during which responses were stable (Figures 3L and 3P). After 60 min postmortem, the vibratory patterns sometimes changed and therefore were not used.

Vibrations in Mice with Altered Bundle Mechanics

To assess the influence of the OHC stereociliary bundles on cochlear mechanics, we compared vibrations measured in WT mice to those from three mutant strains with progressively larger alterations to the integrity of the bundles and/or their attachment to the TM (Figures 4, 5, and 6). Postmortem response curves from all mice were then parameterized (Figure 7; Table S1) to determine whether effects in mutant mice were consistent with reduced transverse partition stiffness (reduced BF, broadened tuning) or reduced longitudinal coupling (sharpened tuning, steeper phase slope). Since two of the mutant strains (*salsa* and $Triobp^{\Delta ex8/\Delta ex8}$) were bred on the C57BL/6J background while the third ($Tecta^{C1509G/C1509G}$) was bred on the CBA/CaJ background, data are reported as percentages of the appropriate WT mean to facilitate comparison across mice (see Table S1 for a summary of the raw data). We report statistical analyses only for the BM data, since the findings were similar for the RL and TM.

(1) salsa Mice: Loss of Tip Links—We first examined *salsa* mice, which progressively lose their stereociliary tip links due to a missense mutation affecting CDH23 (Schwander et al., 2009), an integral tip link protein (Kazmierczak et al., 2007) (Figure 4A). Tip links are required for mechanotransduction, as it is the tension on the tip links during bundle deflection that gates open ion channels. The bundles in *salsa* mice are presumably less stiff, since loss of tip links due to application of 1,2-bis(2-aminophenoxy)ethane-*N,N,N′,N′*-tetraacetic acid (BAPTA) reduces OHC bundle stiffness *in vitro* by ~38% (Beurg et al., 2008). While we found no abnormalities in bundle morphology in phalloidin-labeled, whole-mount cochlear preparations from post-natal day (P)30 *salsa* mice or in cross-sectional images of the cochlear duct obtained with VOCTV in P21–P35 mice (Figures 4B and 4C), vibratory responses measured from the BM, RL, and TM of live *salsa* mice lacked nonlinear gain (Figures 4D–4J). This indicates that the tip links had degenerated by the age of testing, so that mechanotransduction and amplification were impaired.

We compared postmortem vibrations in *salsa* and WT mice (Figures 4K–4P) and found that vibrations from both mice peaked at frequencies near 4.5–5 kHz, with no significant

difference in the BF (Figure 7B) or the intercept 10 dB down from the peak at frequencies below the BF (F_{low}; Figure 7C). However, the high-frequency extent of the responses was significantly reduced in *salsa* mice (by ~9%), as quantified by the intercept 10 dB down from the peak at frequencies above the BF (F_{high}; Figure 7D). To quantify the sharpness of tuning, we divided the BF by the bandwidth 10 dB down from the peak to obtain the Q factor (Q_{10dB}), which was significantly higher in *salsa* mice (by ~15%; Figure 7E). Lastly, we compared the negative slope of the phase curve (in cycles per octave) at the frequency where the phase crossed −1.75 cycles, and found that phase slopes were significantly higher in *salsa* mice (by ~11%; Figure 7F). Elimination of tip links therefore led to traveling waves that excited a narrower spatial region and decayed more rapidly as a function of distance. These effects are consistent with a reduction in longitudinal coupling rather than a reduction in the transverse stiffness of the partition.

(2) Triobp$^{\Delta ex8/\Delta ex8}$ Mice: No Rootlets—We next measured vibrations in *Triobp$^{\Delta ex8/\Delta ex8}$* mice, which fail to develop stereociliary rootlets (Figure 5A) due to a deficiency in actin-bundling proteins TRIOBP-4 and TRIOBP-5 (Kitajiri et al., 2010). As a result, stereociliary bundles in *Triobp$^{\Delta ex8/\Delta ex8}$* mice are 50% less stiff at early post-natal ages (Kitajiri et al., 2010). Because of their increased susceptibility to overstimulation, the bundles exhibit widespread damage by adulthood, which we confirmed with phalloidin-stained, whole-mount preparations (Figure 5B). Similar to our observations in *salsa* mice, we found no abnormalities in cross-sectional images of the cochlear duct obtained with VOCTV (Figure 5C), and vibrations measured in live mice lacked nonlinear gain (Figures 5D–5J). Thus, the bundle degeneration was sufficient to impair mechanotransduction and amplification in *Triobp$^{\Delta ex8/\Delta ex8}$* mice.

As in *salsa* mice, postmortem vibration measurements revealed that the high-frequency extent of vibratory responses was significantly reduced in *Triobp$^{\Delta ex8/\Delta ex8}$* mice (by 12%; Figures 5K–5P and 7D). Reductions in the BF and F_{low} were small and not statistically significant (Figures 7B and 7C). The responses were therefore more sharply tuned in *Triobp$^{\Delta ex8/\Delta ex8}$* mice, with Q_{10dB} values that were significantly higher (by ~14%; Figure 7E). Additionally, phase slopes were significantly steeper in *Triobp$^{\Delta ex8/\Delta ex8}$* mice (by 14%; Figure 7F). Elimination of the stereociliary rootlet and disruption of the bundles therefore produced effects that were primarily consistent with a reduction in longitudinal coupling rather than transverse stiffness.

(3) Tecta$^{C1509G/C1509G}$ Mice: TM Detached—Lastly, we examined vibrations in *Tecta$^{C1509G/C1509G}$* mice (Figure 6A), in which the TM is malformed and lifted off the epithelium so that it does not contact the OHC stereocilia (Xia et al., 2010). Bundle morphology was normal in *Tecta$^{C1509G/C1509G}$* mice (Figure 6B), though the separation of the TM from the RL was evident in cross-sectional images of the cochlear duct obtained with VOCTV (Figure 6C). Consistent with our previous report (Lee et al., 2016), vibratory responses from live *Tecta$^{C1509G/C1509G}$* mice lacked nonlinear gain (Figures 6D–6J). This is presumably because the OHC stereocilia are not efficiently stimulated when they are uncoupled from the TM. Without the load of the TM, the bundle's influence on the partition's passive response should also be reduced.

In line with our findings in *salsa* and *Triobp*$^{\Delta ex8/\Delta ex8}$ mice, comparisons of postmortem vibrations revealed a significant reduction (~18%) in the high-frequency extent of responses in *Tecta*$^{C1509G/C1509G}$ mice (Figures 6K–6P and 7D). However, the BF was also significantly reduced in *Tecta*$^{C1509G/C1509G}$ mice (by ~14%; Figure 7B) and a similar, though non-statistically significant, reduction was observed in F_{low} (Figure 7C). Tuning sharpness was therefore increased by a smaller, non-statistically significant amount (7.87%, $p = 0.071$; Figure 7E). Similarly, phase slopes in *Tecta*$^{C1509G/C1509G}$ were also only ~4% steeper than in WT, a non-statistically significant difference (Figure 7F). Since the lower BF indicates a reduction in transverse partition stiffness, the small effects on tuning sharpness and phase slope in *Tecta*$^{C1509G/C1509G}$ mice could be explained by the combined effects of reduced longitudinal coupling and reduced transverse stiffness, which have opposing effects on these parameters. Our findings in *Tecta*$^{C1509G/C1509G}$ mice are therefore compatible with the notion that the stereocilia contribute to longitudinal coupling and further suggest that the attachment of the TM contributes to the transverse stiffness of the partition in WT mice. In contrast, bundle stiffness alone appears to contribute little to the transverse stiffness.

DISCUSSION

Here, we demonstrated that the OHC stereociliary bundles and TM directly influence passive cochlear mechanics. In mice with altered bundle stiffness (*salsa* and *Triobp*$^{\Delta ex8/\Delta ex8}$ mice), the high-frequency extent of the vibratory responses was reduced, tuning was sharpened, and the vibratory phase curve sloped more steeply. These effects are all consistent with a reduction in longitudinal coupling within the cochlear partition (Allen and Sondhi, 1979; Eze and Olson, 2011; Meaud and Grosh, 2010; Wickesberg and Geisler, 1986). In contrast, when the TM was detached from the stereocilia (as in *Tecta*$^{C1509G/C1509G}$ mice), there was an overall downward shift of the frequency response, though the shift was largest at high frequencies, consistent with the combined effects of reduced longitudinal coupling and reduced transverse stiffness. This finding implies that the TM contributes substantially more to the transverse stiffness of the partition than do the bundles. Since reductions in the mass of the TM or cochlear partition in *Tecta*$^{C1509G/C1509G}$ mice would increase rather than decrease the observed BF, the altered frequency response in these mice cannot be due to a change in mass.

Importantly, the mutations in each of the mouse models affected not only the vibrations of the TM and RL but also those of the BM. Thus, the OHC bundles and TM contribute to the passive mechanical response of the entire cochlear partition. Specifically, by spreading excitation to more apical locations, the OHC bundles and TM enhance the passive response of a given location to higher-frequency stimuli. *In vivo*, this would increase the input to the active OHC-mediated feedback process for frequencies near the location's CF, thus facilitating cochlear amplification.

Stereociliary Bundle Stiffness Confers Longitudinal Coupling

Through their attachment to the TM, the OHC stereocilia provide bidirectional coupling of the mechanical properties of the TM and the organ of Corti-BM complex. These structures have all been demonstrated to have longitudinal stiffness (Abnet and Freeman, 2000; Naidu

and Mountain, 2001), such that the OHC bundles may aid in establishing longitudinal coupling for the cochlear partition as a whole. The bundles themselves could also contribute longitudinal stiffness via the top connectors that link adjacent stereocilia within each row (Goodyear et al., 2005). However, this contribution may be small, as bundle stiffness in the direction orthogonal to the tip links (in the longitudinal direction along the partition) is likely less than the radial bundle stiffness (Howard and Hudspeth, 1987).

Longitudinal coupling within the TM has been proposed to be particularly important in controlling the spread of cochlear excitation (Ghaffari et al., 2007, 2010; Meaud and Grosh, 2010; Russell et al., 2007; Sellon et al., 2015). For instance, BM responses are more sharply tuned in a mutant mouse (*Tectb*$^{-/-}$) where the TM's mechanics are altered due to disruption of its striated sheet matrix (Russell et al., 2007). Isolated segments of mouse TM have also been demonstrated to support longitudinally propagating, radial displacement waves (Ghaffari et al., 2007). The space constants of these waves are sensitive to the material properties of the TM and correlate with auditory phenotypes of mutant mice with abnormal TMs (Ghaffari et al., 2010; Sellon et al., 2014). The OHC stereociliary bundles are, of course, in an ideal position to both sense and modify radial motions of the TM. Our findings are therefore consistent with a role for the TM in longitudinal coupling and provide evidence that coupling between the bundles and TM influences the apical extent of wave travel within the cochlea.

Contribution to the Transverse Stiffness of the Cochlear Partition

The lack of significant shifts in the BF in *salsa* and *Triobp*$^{\Delta ex8/\Delta ex8}$ mice indicates that bundle stiffness contributes little to the transverse stiffness of the partition in the mouse cochlear apex. If a given location along the partition can be approximated by a spring-mass system, its BF is proportional to the square root of the transverse stiffness. Thus, we estimate that partition stiffness was reduced by only 1.1% in *salsa* mice and 8.2% in *Triobp*$^{\Delta ex8/\Delta ex8}$ mice. These findings contrast with the ~25% reduction in partition stiffness observed in an *in vitro* preparation of the gerbil cochlear apex after elimination of the tip links with BAPTA application (Chan and Hudspeth, 2005). In this *in vitro* preparation, eliminating tip links not only reduced the BF of the partition but also broadened its tuning, which we did not observe in *salsa* or *Triobp*$^{\Delta ex8/\Delta ex8}$ mice.

These different findings may be due to the species used, as the apex in gerbil responds to much lower frequencies than that in the mouse. Apical mechanical responses in gerbil or guinea pig are indeed distinct from those at the base in these species (Cooper and Rhode, 1995; Dong and Cooper, 2006; Recio-Spinoso and Oghalai, 2017), and the relative stiffnesses of the bundles and surrounding structures may differ (Abnet and Freeman, 2000; Gu et al., 2008; Zwislocki and Cefaratti, 1989). Additionally, while we focused on passive, just-postmortem responses, the *in vitro* gerbil preparation maintained a degree of nonlinear amplification, which must have been lost after breaking the tip links. It is also possible that tip links had not fully degenerated in *salsa* mice at the age tested, as stereociliary "tenting" —thought to be due to tip-link-mediated tension—has been observed in the apex of *salsa* mice at P21 (Schwander et al., 2009). However, data from *Triobp*$^{\Delta ex8/\Delta ex8}$ mice likely

provide an upper bound for the effect of tip link loss, as the overall integrity of the bundles was severely affected in these mice.

It may seem paradoxical that the OHC bundles must be sufficiently stiff to couple the mechanical properties of the TM and organ of Corti-BM complex and confer longitudinal coupling but appear to contribute little to the transverse stiffness of the partition. However, modeling results suggest that small amounts of longitudinal coupling can strongly alter the high-frequency slopes of the vibratory gain and phase curves (Allen and Sondhi, 1979). If the bundles contribute an equivalently small amount to both the longitudinal and transverse stiffnesses of the cochlear partition, the effects of reducing bundle stiffness may be dominated by the reduction in longitudinal coupling, as observed in *salsa* and $Triobp^{\Delta ex8/\Delta ex8}$ mice. Larger stiffness changes may be required before the dominant effect resembles that of reduced transverse stiffness. For instance, the BF was reduced in $Tecta^{C1509G/C1509G}$ mice, in which the TM was detached from the organ of Corti, while evidence for reduced longitudinal coupling was less strong. Similar findings (i.e., evidence for reduced partition stiffness but not longitudinal coupling) have been reported for BM vibrations in gerbil cochleae treated with neomycin, which largely eliminated OHCs and supporting cells, thus uncoupling the TM from the BM (Eze and Olson, 2011).

Mechanical Role of the TM

The lower BF in $Tecta^{C1509G/C1509G}$ mice suggests that, together with the OHC bundles, the TM contributes 25.7% to the transverse partition stiffness. This value is comparable to the ~30% stiffness reduction found for the *in vitro* gerbil preparation after removal of the TM (Chan and Hudspeth, 2005). Since altering bundle stiffness alone did not produce similar effects, the TM must be considerably stiffer than the bundles in the apex of the mouse cochlea. This conclusion is consistent with the mechanical properties of isolated TM segments from the mouse apex (Abnet and Freeman, 2000; Gu et al., 2008). While a reduction in transverse stiffness should also increase the partition's vibratory magnitude, we did not observe this effect with our semi-radial motion measurements. However, increased vibration magnitudes in $Tecta^{C1509G/C1509G}$ mice were found in our previous report (Lee et al., 2016), in which the transverse and radial motions were measured. Reductions in longitudinal coupling alone are predicted to have little effect on passive vibration magnitudes (Meaud and Grosh, 2010).

The TM has been proposed to contribute to a radial resonance via its mass and its attachments to the spiral limbus and OHC stereocilia (Allen, 1980; Allen and Fahey, 1993; Gummer et al., 1996; Zwislocki, 1980). This resonance is thought to produce a secondary peak in BM sensitivity 0.5 octaves below the CF at the base of the mouse cochlea, a feature that is absent in mice with certain TM mutations (Legan et al., 2000). However, there is little evidence for this second resonance in vibrations from the mouse cochlear apex, possibly due to basal-to-apical increases in TM damping (Zwislocki, 2002) or longitudinal coupling (Lukashkin et al., 2010), which would reduce the effects of a parallel TM resonance. Interestingly, while the BFs of BM and TM vibrations in $Tecta^{C1509G/C1509G}$ mice were within 10% of one another, TM vibrations exhibited a second magnitude peak near 10 kHz, the CF of this cochlear location in live WT mice (Figures 6G and 6M). While this could

indicate that the TM has a natural resonance near the CF, the TM in *Tecta*$^{C1509G/C1509G}$ mice is malformed and detached from the OHC stereocilia. The relevance of this peak to normal cochlear mechanics *in vivo* is therefore unclear.

Limitations of Postmortem Measurements

We focused our analyses on postmortem measurements, since any comparisons with live WT mice were confounded by the effects of amplification. This approach may have misrepresented the influence of bundle stiffness *in vivo* if a portion of this stiffness depends on transduction currents or is otherwise metabolically dependent. For instance, tension on the tip links is thought to be actively regulated by myosin motors (Assad and Corey, 1992) and, thus, is likely decreased in WT mice after death.

Implications for Active Mechanics *In vivo*

We conclude that the passive stiffness of the OHC stereociliary bundles extends the apical spread of excitation within the cochlea, likely via interactions with the TM. Active force generation by the bundles *in vivo* could contribute to this longitudinal coupling, further enhancing the response to near-CF stimuli at a given cochlear location. Both the passive and active properties of the bundles may therefore play a direct mechanical role in the cochlear amplification process, in addition to the forces provided by OHC somatic motility.

EXPERIMENTAL PROCEDURES

Mice

Mutant mice and WT controls (C57BL/6J for *salsa* and *Triobp*$^{\Delta ex8/\Delta ex8}$ mice; CBA/CaJ for *Tecta*$^{C1509G/C1509G}$ mice) were bred onsite. Experiments were performed on equal numbers of male and female adult mice (P21–P35). The mean ± SEM for the experimental test age was 29.3 ± 0.51 days across all mice (n = 50, including 10 mice for each strain). Prior morphological assessments and demonstrations of moderately to severely elevated auditory brainstem response thresholds by P21–P28 in all three mutant strains suggest that the integrity of the stereocilia or their attachment to the TM were affected by the ages tested here (Kitajiri et al., 2010; Schwander et al., 2009; Xia et al., 2010). We further assessed stereociliary integrity in each strain by examining phalloidin-stained cochlear whole-mount preparations from P30 mice. All procedures were performed at Stanford University and were approved by Stanford's Institutional Animal Care and Use Committee.

Cochlear Whole-Mount Immunostaining

Excised cochleae were fixed with 4% paraformaldehyde (PFA) at room temperature for 1 hr and microdissected to reveal the organ of Corti. Specimens were then washed with PBS containing 0.01% Triton X-100 (PBST) (pH 7.4) and immunostained with Alexa Fluor 488 Phalloidin 1:200 (A12379, Thermo Fisher Scientific, Waltham, MA, USA) for 30 min. After washing with PBS, specimens were mounted in anti-fade Fluorescence Mounting Medium (DAKO, Carpinteria, CA, USA) and coverslipped. Images were acquired with a LSM 700 confocal microscope (Zeiss, Thornwood, NY, USA) using a 63× objective. Image stacks were recut at angles appropriate for visualizing either the OHC or IHC stereocilia using Fiji (ImageJ) software, and the resulting images were stitched together.

Cochlear Vibration Measurements

Mice were anesthetized with ketamine (80–100 mg/kg) and xylazine (5–10 mg/kg) and placed on a heating pad to maintain a core temperature of 37.6°C. Supplemental doses of anesthesia were provided to maintain areflexia. After fixing the skull to a custom head-holder with dental cement, a ventrolateral surgical approach was used to access the left middle ear bulla. The bone below the tympanic annulus was then widely opened to allow visualization of the otic capsule bone and the middle ear ossicles. The pinna and cartilaginous external ear canal were partially dissected, and a sound source was positioned within a few millimeters of the eardrum.

We imaged and measured vibrations from within the apical cochlear turn using VOCTV, as described previously (Gao et al., 2014; Lee et al., 2015, 2016). Briefly, the custom-built system consisted of a broadband swept source (MEMS-VCSEL, Thorlabs) with a center wavelength of 1,300 nm, a bandwidth of 100 nm, and a 200-kHz sweep rate, as well as a dual-balanced photodetector (WL-BPD600MA, WieserLabs), and a high-speed digitizer (NI-5761, National Instruments). The source beam was scanned across the preparation using a 2D voice coil mirror housed in an adaptor that was attached to the bottom of the dissecting microscope (Stemi-2000, Carl Zeiss).

After obtaining 2D cross-sectional images of the cochlea, vibrations were measured from single voxels representing points on the BM, TM, and RL at a location approximately one half-turn from the apex. To reduce variation in the location studied, we oriented the equipment and mouse's head as similarly as possible across experiments. Measurement points always corresponded to local maxima in the intensity versus depth function for a given x-coordinate. This maximized the vibratory signal-to-noise ratio and minimized distortions due to signal competition from adjacent locations (Ellerbee and Izatt, 2007; Lin et al., 2017). Sound stimuli were digitally generated and presented via a speaker (MDR EX37B, Sony) that was fixed to the head-holder and positioned close to the eardrum. Vibrations were measured in response to 200-ms pure tones swept from 2 to 14 kHz in 0.5 kHz steps, and from 10 to 80 dB SPL in 10 dB steps. Stimuli were calibrated prior to each experiment using a Brüel & Kjær 1/4" microphone (Type 4939).

After completing *in vivo* measurements, mice were sacrificed via anesthetic overdose, and measurements were repeated 10–60 min postmortem. Time of death was determined by the absence of breathing, heartbeat, and other movements. Lastly, the head was rotated to visualize the middle ear ossicles, and vibrations were recorded from the orbicular apophysis of the malleus. This allowed normalization of the displacements of the cochlear structures to those of the ossicular chain so that the cochlear gain per unit input could be calculated. All vibratory data shown had displacement magnitudes at least 3 SDs above the mean measurement noise floor, as computed from frequency bins within ±200–300 Hz of the stimulus frequency.

Statistical Reporting

Vibratory responses were parameterized to assess whether effects observed in mutant mice were consistent with reduced transverse partition stiffness or reduced longitudinal coupling.

Vibratory data were extrapolated to 1 kHz to facilitate quantification of the response bandwidth, allowing estimates in all mice except for one WT C57BL/6J control. Slopes of the vibratory phase versus frequency curves could be computed for all mice at the −1.75 cycle phase intercept except for two *Tecta*$^{C1509G/C1509G}$ mice, in which the vibratory magnitudes were below the noise floor at this intercept. Differences between each mutant strain and its WT control were assessed with unpaired t tests. Differences across mutants were assessed with one-way ANOVA and Tukey post hoc comparisons, after expressing all values as a percentage of the appropriate mean WT value. p values < 0.05 were considered significant. Reported values are the mean ± SEM.

Supplementary Material

Refer to Web version on PubMed Central for supplementary material.

ACKNOWLEDGMENTS

This work was supported by NIDCD/NIH grants DC014450 and DC013774 to J.S.O.; DC016211 to J.B.D.; P30DC010363 to Stanford University; and funds from the NIDCD/NIH Intramural Research Program DC000039–20 to Thomas B. Friedman (for I.A.B.).

REFERENCES

Abnet CC, and Freeman DM (2000). Deformations of the isolated mouse tectorial membrane produced by oscillatory forces. Hear. *Res.* 144, 29–46. [PubMed: 10831863]

Allen JB (1980). Cochlear micromechanics–a physical model of transduction. J. Acoust. Soc. Am 68, 1660–1670. [PubMed: 7462465]

Allen JB, and Fahey PF (1993). A second cochlear-frequency map that correlates distortion product and neural tuning measurements. J. Acoust. Soc. Am 94, 809–816. [PubMed: 8370887]

Allen JB, and Sondhi MM (1979). Cochlear macromechanics: time domain solutions. J. Acoust. Soc. Am 66, 123–132. [PubMed: 489828]

Assad JA, and Corey DP (1992). An active motor model for adaptation by vertebrate hair cells. J. Neurosci 12, 3291–3309. [PubMed: 1527581]

Beurg M, Nam J-H, Crawford A, and Fettiplace R (2008). The actions of calcium on hair bundle mechanics in mammalian cochlear hair cells. Biophys. J 94, 2639–2653. [PubMed: 18178649]

Brownell WE, Bader CR, Bertrand D, and de Ribaupierre Y (1985). Evoked mechanical responses of isolated cochlear outer hair cells. Science 227, 194–196. [PubMed: 3966153]

Chan DK, and Hudspeth AJ (2005). Mechanical responses of the organ of corti to acoustic and electrical stimulation in vitro. Biophys. J 89, 4382–4395. [PubMed: 16169985]

Cooper NP (2000). Radial variation in the vibrations of the cochlear partition In Recent Developments in Auditory Mechanics, Wada H, Takasaka T, Ikeda K, Ohyama K, and Koike T, eds. (World Scientific), pp. 109–115.

Cooper NP, and Rhode WS (1995). Nonlinear mechanics at the apex of the guinea-pig cochlea. Hear. Res 82, 225–243. [PubMed: 7775288]

Dallos P, Wu X, Cheatham MA, Gao J, Zheng J, Anderson CT, Jia S, Wang X, Cheng WHY, Sengupta S, et al. (2008). Prestin-based outer hair cell motility is necessary for mammalian cochlear amplification. Neuron 58, 333–339. [PubMed: 18466744]

Dong W, and Cooper NP (2006). An experimental study into the acousto-mechanical effects of invading the cochlea. J. R. Soc. Interface 3, 561–571. [PubMed: 16849252]

Ellerbee AK, and Izatt JA (2007). Phase retrieval in low-coherence interferometric microscopy. Opt. Lett 32, 388–390. [PubMed: 17356662]

Eze N, and Olson ES (2011). Basilar membrane velocity in a cochlea with a modified organ of Corti. Biophys. J 100, 858–867. [PubMed: 21320429]

Gao SS, Wang R, Raphael PD, Moayedi Y, Groves AK, Zuo J, Applegate BE, and Oghalai JS (2014). Vibration of the organ of Corti within the cochlear apex in mice. J. Neurophysiol 112, 1192–1204. [PubMed: 24920025]

Geisler CD (1998). From Sound to Synapse (Oxford University Press).

Ghaffari R, Aranyosi AJ, and Freeman DM (2007). Longitudinally propagating traveling waves of the mammalian tectorial membrane. Proc. Natl. Acad. Sci. USA 104, 16510–16515. [PubMed: 17925447]

Ghaffari R, Aranyosi AJ, Richardson GP, and Freeman DM (2010). Tectorial membrane travelling waves underlie abnormal hearing in Tectb mutant mice. Nat. Commun 1, 96. [PubMed: 20981024]

Goodyear RJ, Marcotti W, Kros CJ, and Richardson GP (2005). Development and properties of stereociliary link types in hair cells of the mouse cochlea. J. Comp. Neurol 485, 75–85. [PubMed: 15776440]

Gu JW, Hemmert W, Freeman DM, and Aranyosi AJ (2008). Frequencydependent shear impedance of the tectorial membrane. Biophys. J 95, 2529–2538. [PubMed: 18515382]

Guinan JJ, Jr. (2012). How are inner hair cells stimulated? Evidence for multiple mechanical drives. Hear. Res 292, 35–50. [PubMed: 22959529]

Gummer AW, Hemmert W, and Zenner HP (1996). Resonant tectorial membrane motion in the inner ear: its crucial role in frequency tuning. Proc. Natl. Acad. Sci. USA 93, 8727–8732. [PubMed: 8710939]

Howard J, and Hudspeth AJ (1987). Mechanical relaxation of the hair bundle mediates adaptation in mechanoelectrical transduction by the bullfrog's saccular hair cell. Proc. Natl. Acad. Sci. USA 84, 3064–3068. [PubMed: 3495007]

Hu X, Evans BN, and Dallos P (1999). Direct visualization of organ of corti kinematics in a hemicochlea. J. Neurophysiol 82, 2798–2807. [PubMed: 10561446]

Hudspeth AJ (2014). Integrating the active process of hair cells with cochlear function. Nat. Rev. Neurosci 15, 600–614. [PubMed: 25096182]

Kazmierczak P, Sakaguchi H, Tokita J, Wilson-Kubalek EM, Milligan RA, Mu€ller U, and Kachar B (2007). Cadherin 23 and protocadherin 15 interact to form tip-link filaments in sensory hair cells. Nature 449, 87–91. [PubMed: 17805295]

Kennedy HJ, Crawford AC, and Fettiplace R (2005). Force generation by mammalian hair bundles supports a role in cochlear amplification. Nature 433, 880–883. [PubMed: 15696193]

Kitajiri S, Sakamoto T, Belyantseva IA, Goodyear RJ, Stepanyan R, Fujiwara I, Bird JE, Riazuddin S, Riazuddin S, Ahmed ZM, et al. (2010). Actin-bundling protein TRIOBP forms resilient rootlets of hair cell stereocilia essential for hearing. Cell 141, 786–798. [PubMed: 20510926]

Konishi T, Butler RA, and Fernandez C (1961). Effect of anoxia on cochlear potentials. J. Acoust. Soc. Am 33, 349–356.

Lee HY, Raphael PD, Park J, Ellerbee AK, Applegate BE, and Oghalai JS (2015). Noninvasive in vivo imaging reveals differences between tectorial membrane and basilar membrane traveling waves in the mouse cochlea. Proc. Natl. Acad. Sci. USA 112, 3128–3133. [PubMed: 25737536]

Lee HY, Raphael PD, Xia A, Kim J, Grillet N, Applegate BE, Ellerbee Bowden AK, and Oghalai JS (2016). Two-dimensional cochlear micromechanics measured in vivo demonstrate radial tuning within the mouse organ of Corti. J. Neurosci 36, 8160–8173. [PubMed: 27488636]

Legan PK, Lukashkina VA, Goodyear RJ, Ko¨ ssi M, Russell IJ, and Richardson GP (2000). A targeted deletion in alpha-tectorin reveals that the tectorial membrane is required for the gain and timing of cochlear feedback. Neuron 28, 273–285. [PubMed: 11087000]

Liberman MC, Gao J, He DZZ, Wu X, Jia S, and Zuo J (2002). Prestin is required for electromotility of the outer hair cell and for the cochlear amplifier. Nature 419, 300–304. [PubMed: 12239568]

Lim DJ (1986). Functional structure of the organ of Corti: a review. Hear. Res 22, 117–146. [PubMed: 3525482]

Lin NC, Hendon CP, and Olson ES (2017). Signal competition in optical coherence tomography and its relevance for cochlear vibrometry. J. Acoust. Soc. Am 141, 395–405. [PubMed: 28147569]

Lukashkin AN, Richardson GP, and Russell IJ (2010). Multiple roles for the tectorial membrane in the active cochlea. Hear. Res 266, 26–35. [PubMed: 19853029]

Meaud J, and Grosh K (2010). The effect of tectorial membrane and basilar membrane longitudinal coupling in cochlear mechanics. J. Acoust. Soc. Am 127, 1411–1421. [PubMed: 20329841]

Naidu RC, and Mountain DC (2001). Longitudinal coupling in the basilar membrane. J. Assoc. Res. Otolaryngol 2, 257–267. [PubMed: 11669398]

Neely ST (1993). A model of cochlear mechanics with outer hair cell motility. J. Acoust. Soc. Am 94, 137–146. [PubMed: 8354757]

Oghalai JS (2004). The cochlear amplifier: augmentation of the traveling wave within the inner ear. Curr. Opin. Otolaryngol. Head Neck Surg 12, 431–438. [PubMed: 15377957]

Olson ES, Duifhuis H, and Steele CR (2012). Von Békésy and cochlear mechanics. Hear. Res 293, 31–43. [PubMed: 22633943]

Recio-Spinoso A, and Oghalai JS (2017). Mechanical tuning and amplification within the apex of the guinea pig cochlea. J. Physiol 595, 4549–4561. [PubMed: 28382742]

Ren T, He W, and Kemp D (2016). Reticular lamina and basilar membrane vibrations in living mouse cochleae. Proc. Natl. Acad. Sci. USA 113, 9910–9915. [PubMed: 27516544]

Richter C-P, Emadi G, Getnick G, Quesnel A, and Dallos P (2007). Tectorial membrane stiffness gradients. Biophys. J 93, 2265–2276. [PubMed: 17496047]

Robles L, and Ruggero MA (2001). Mechanics of the mammalian cochlea. Physiol. Rev 81, 1305–1352. [PubMed: 11427697]

Russell IJ, and Cowley EM (1983). The influence of transient asphyxia on receptor potentials in inner hair cells of the guinea pig cochlea. Hear. Res 11, 373–384. [PubMed: 6630089]

Russell IJ, Legan PK, Lukashkina VA, Lukashkin AN, Goodyear RJ, and Richardson GP (2007). Sharpened cochlear tuning in a mouse with a genetically modified tectorial membrane. Nat. Neurosci 10, 215–223. [PubMed: 17220887]

Sadanaga M, and Morimitsu T (1995). Development of endocochlear potential and its negative component in mouse cochlea. Hear. Res 89, 155–161. [PubMed: 8600121]

Schwander M, Xiong W, Tokita J, Lelli A, Elledge HM, Kazmierczak P, Sczaniecka A, Kolatkar A, Wiltshire T, Kuhn P, et al. (2009). A mouse model for nonsyndromic deafness (DFNB12) links hearing loss to defects in tip links of mechanosensory hair cells. Proc. Natl. Acad. Sci. USA 106, 5252–5257. [PubMed: 19270079]

Sellon JB, Ghaffari R, Farrahi S, Richardson GP, and Freeman DM (2014). Porosity controls spread of excitation in tectorial membrane traveling waves. Biophys. J 106, 1406–1413. [PubMed: 24655516]

Sellon JB, Farrahi S, Ghaffari R, and Freeman DM (2015). Longitudinal spread of mechanical excitation through tectorial membrane traveling waves. Proc. Natl. Acad. Sci. USA 112, 12968–12973. [PubMed: 26438861]

Shoelson B, Dimitriadis EK, Cai H, Kachar B, and Chadwick RS (2004). Evidence and implications of inhomogeneity in tectorial membrane elasticity. Biophys. J 87, 2768–2777. [PubMed: 15454468]

Strelioff D, Flock A, and Minser KE (1985). Role of inner and outer hair cells in mechanical frequency selectivity of the cochlea. Hear. Res 18, 169–175. [PubMed: 4044418]

von Békésy G (1960). Experiments in Hearing (McGraw-Hill).

Wickesberg RE, and Geisler CD (1986). Longitudinal stiffness coupling in a 1-dimensional model of the peripheral ear In Peripheral Auditory Mechanisms, Allen JB, Hall JL, Hubbard A, Neely ST, and Tubis A, eds. (Springer), pp. 113–120.

Xia A, Gao SS, Yuan T, Osborn A, Bress A, Pfister M, Maricich SM, Pereira FA, and Oghalai JS (2010). Deficient forward transduction and enhanced reverse transduction in the alpha tectorin C1509G human hearing loss mutation. Dis. Model. Mech 3, 209–223. [PubMed: 20142329]

Zwislocki JJ (1980). Theory of cochlear mechanics. Hear. Res 2, 171–182.

Zwislocki JJ (2002). Auditory Sound Transmission: An Autobiographical Perspective (Lawrence Erlbaum Associates).

Zwislocki JJ, and Cefaratti LK (1989). Tectorial membrane. II: stiffness measurements in vivo. Hear. Res 42, 211–227. [PubMed: 2606804]

Highlights

- Reducing stereociliary bundle stiffness sharpens the tuning of cochlear vibrations
- Detachment of the tectorial membrane from the stereocilia has a similar effect
- Stereociliary bundles facilitate the spread of excitation toward the cochlear apex

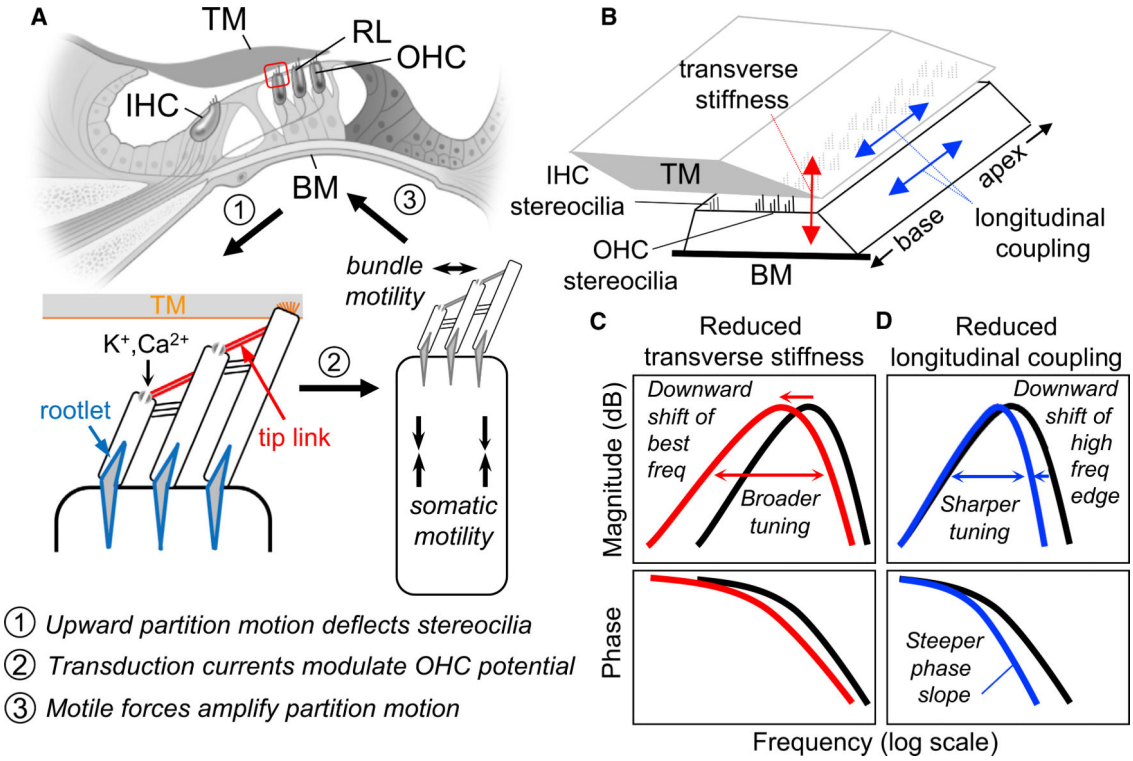

Figure 1. Role of the OHC Stereociliary Bundle in Active and Passive Cochlear Mechanics

(A) Cartoons illustrating that OHC mechanotransduction leads to amplification of cochlear vibrations. Upward motion of the cochlear partition (top) deflects the stereociliary bundle in the excitatory direction (lower left). Tension on the tip links gates open ion channels, resulting in inward K^+ and Ca^{2+} currents and modulation of the transmembrane potential. Motile forces generated by the OHC soma and possibly by the bundle amplify the motion of the partition (lower right). In mice with mutations affecting the tip links, rootlets, or stereocilia-TM attachment (highlighted in lower left), amplification is disrupted due to the abolishment of transduction currents and/or impairment of the bundle. In these mice, the influence of these bundle components/properties on the partition's passive mechanics can be studied.

(B) Schematic illustrating that OHC bundle stiffness may contribute to the transverse stiffness of the partition (red arrow) and the degree of mechanical coupling along its length. OHC stereocilia may confer longitudinal coupling by connecting the organ of Corti-BM complex to the TM, both of which have longitudinal stiffness (blue arrows).

(C and D) Predicted effects of reducing bundle stiffness on vibratory magnitude and phase versus frequency patterns obtained at a single cochlear location.

(C) Reducing transverse partition stiffness would shift vibratory response patterns to lower frequencies and broaden their tuning (red curves).

(D) Reducing longitudinal coupling would primarily reduce the high-frequency extent of the magnitude and phase curves, sharpen tuning, and increase the negative slope of the phase versus frequency curve at high frequencies (blue curves).

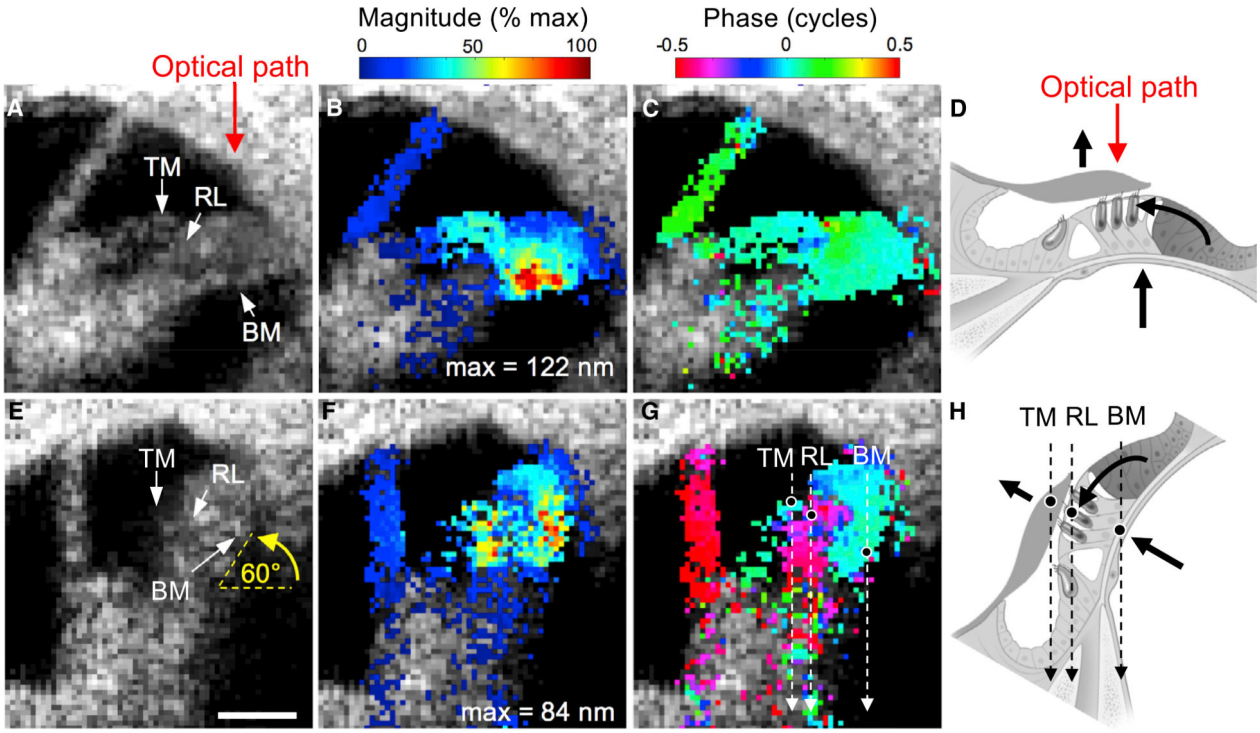

Figure 2. Imaging and Measurement of Semi-radial Vibrations from the Mouse Cochlea *In vivo* Using VOCTV

(A and E) Cross-sectional images obtained from a live WT mouse cochlea with the BM oriented so that its transverse motion was in line with the optical path (A) or with the BM oriented at a ~60° angle so that the semi-radial motion of the structures was measured (E). We measured vibrations using the latter orientation, as this facilitated the identification of measurement points on the BM, RL, and TM based on their different response phases. Scale bar, 100 μm.

(B, C, F, and G) Displacement magnitudes (B and F) and phases (C and G) are indicated in pseudocolor for responses to a 5 kHz, 80 dB SPL tone, with the head in each orientation. Transverse displacements of the cochlear structures were largely in phase (C), while the semi-radial motion of the RL was out of phase with TM and BM motion (G). For clarity, vibratory data are shown only for pixels with an image intensity at least 15% of the maximum.

(D and H) Cartoons illustrating that anti-phasic RL motion results from the inward pivoting of the RL when the BM moves up (D). With the head rotated, this inward motion translates into a downward motion with respect to the optical path (H).

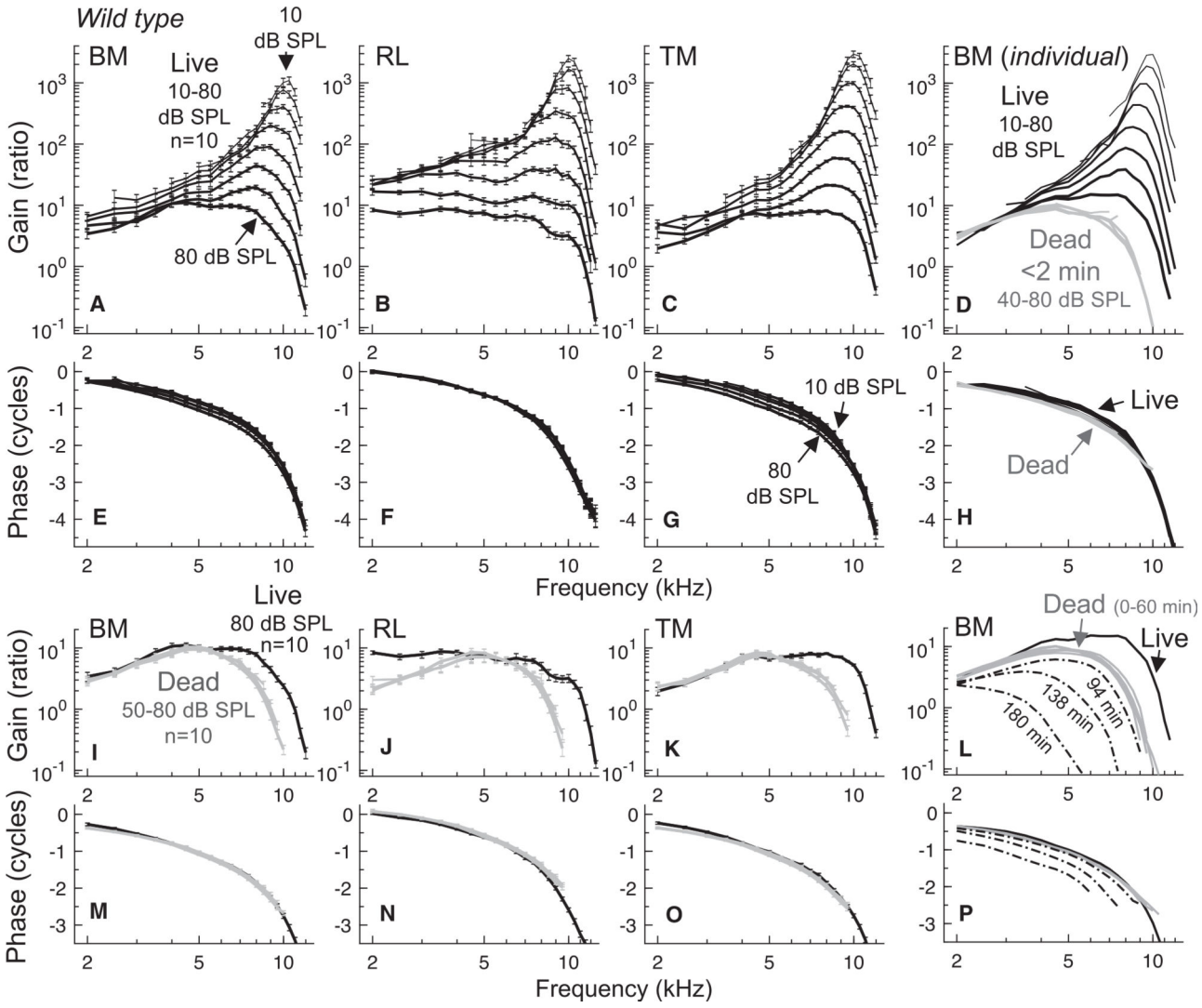

Figure 3. Vibrations in WT Mice

(A–C and E–G) Average vibratory gains (A–C) and phases (E–G) of the BM, RL, and TM, respectively, from 10 live WT C57BL/6J mice. Response curves for the lowest and highest stimulus levels used are indicated in (A) and (G). Gains were calculated by normalizing the displacement of each structure to that of the ossicular chain. Gains in live WT mice were highly dependent on stimulus level (i.e., nonlinear), with maximal gain for low stimulus levels near the CF (~10 kHz).Phases were also level dependent, particularly for the TM (G).

(D and H) BM gain (D) and phase (H) curves for one WT mouse both alive (black curves) and <2 min after death (gray curves). Vibrations became linear after death, as indicated by the overlapping gain curves for 40 to 80 dB SPL stimuli.

(I–K and M–O) Average vibratory gains (I–K) and phases (M–O) of the BM, RL, and TM, respectively, from WT mice obtained 10–60 min postmortem for 50 to 80 dB SPL stimuli. Live WT data for 80 dB SPL stimuli are shown for comparison.

(L and P) BM responses to 80 dB SPL stimuli obtained in one WT mouse alive (black curve), 0–60 min after death (gray curves), and at various times afterward (dotted curves). Responses were stable for up to 60 min. By 90 min postmortem, vibratory magnitudes

tended to be reduced, and the gain (L) and phase (P) curves were shifted downward in frequency, similar to postmortem effects observed in the guinea pig cochlea by Cooper (2000). These effects were possibly due to a decline in the stiffness of the cochlear partition after death.

Error bars for average data indicate SEM.

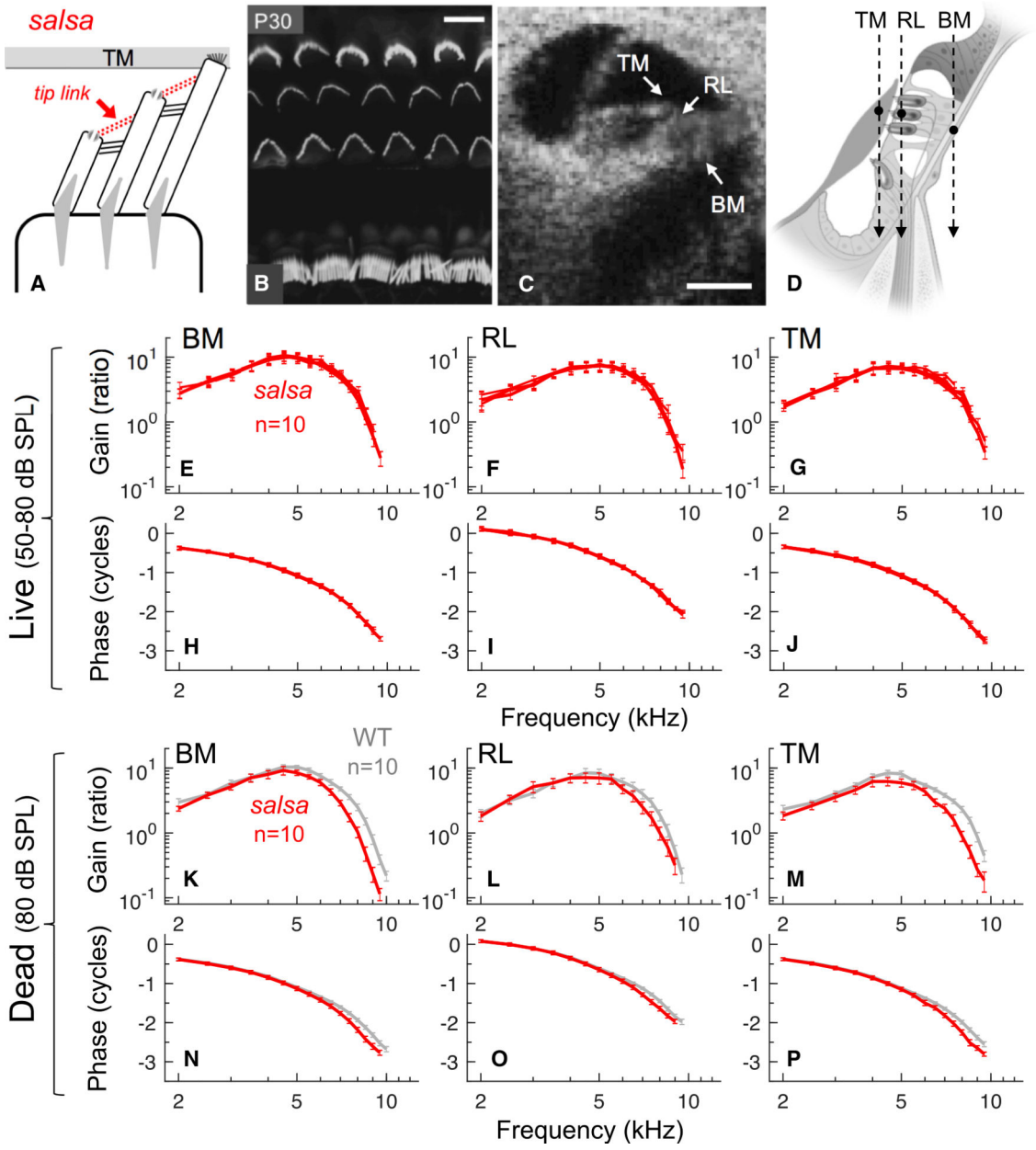

Figure 4. Vibrations in Mice with Progressive Tip Link Loss

(A) Cartoon highlighting that tip links are lost in *salsa* mice.

(B) Phalloidin-stained whole-mount image from the apical turn of a P30 *salsa* mouse cochlea showing grossly normal bundle morphology. Scale bar, 10 μm.

(C) Cross-sectional image of the apical cochlear duct from a *salsa* mouse (obtained with VOCTV) revealing no obvious anatomical abnormalities. Scale bar, 100 mm. For clarity, the image shown was obtained with the BM in a more horizontal orientation.

(D) Schematic illustrating the orientation used in measuring the semi-radial vibrations of the BM, RL, and TM.

(E–J) Average vibratory gains (E–G) and phases (H–J) of the BM, RL, and TM, respectively, from live *salsa* mice (n = 10). Gain curves for 50 to 80 dB SPL stimuli overlapped, indicating passive, linear gain and the absence of cochlear amplification.
(K–P) Average vibratory gains (K–M) and phases (N–P) of the BM, RL, and TM, respectively, from dead *salsa* mice and dead WT C57BL/6J mice for 80 dB SPL stimuli (n = 10 each). The high-frequency extent of the gain and phase curves was reduced in *salsa* mice. Error bars indicate SEM.

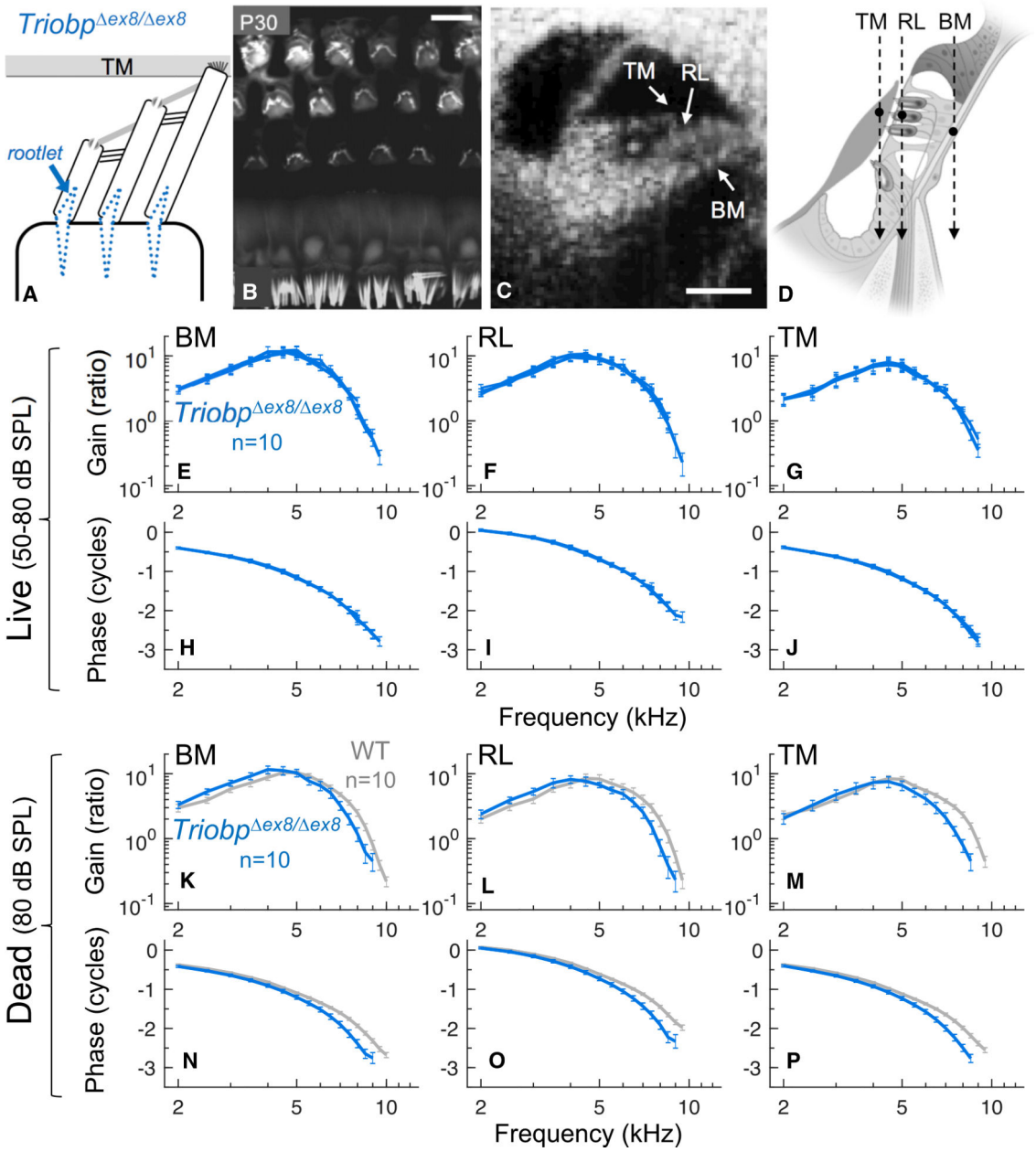

Figure 5. Vibrations in Mice with No Stereociliary Rootlet and Progressive Bundle Degeneration

(A) Cartoon illustrating that *Triobp*$^{\Delta ex8/\Delta ex8}$ mice lack a stereociliary rootlet.

(B) Phalloidin-stained whole-mount image from the apical turn of a P30 *Triobp*$^{\Delta ex8/\Delta ex8}$ mouse cochlea showing substantial bundle degeneration. Scale bar, 10 μm.

(C) Cross-sectional image of the apical cochlear duct from a *Triobp*$^{\Delta ex8/\Delta ex8}$ mouse with the BM oriented horizontally. Scale bar, 100 μm.

(D) Schematic showing the orientation of the structures used for the semi-radial vibration measurements.

(E–J) Average vibratory gains (E–G) and phases (H–J) of the BM, RL, and TM, respectively, from live *Triobp*$^{\Delta ex8/\Delta ex8}$ mice (n = 10) demonstrating linear gain and no cochlear amplification.

(K–P) Average vibratory gains (K–M) and phases (N–P) of the BM, RL, and TM, respectively, from dead *Triobp*$^{\Delta ex8/\Delta ex8}$ mice and dead WT C57BL/6J mice for 80 dB SPL stimuli (n = 10 each). The high-frequency extent of the gain and phase curves was reduced in *Triobp*$^{\Delta ex8/\Delta ex8}$ mice, with only a slight shift evident in the low-frequency portion of the curves.

Error bars indicate SEM.

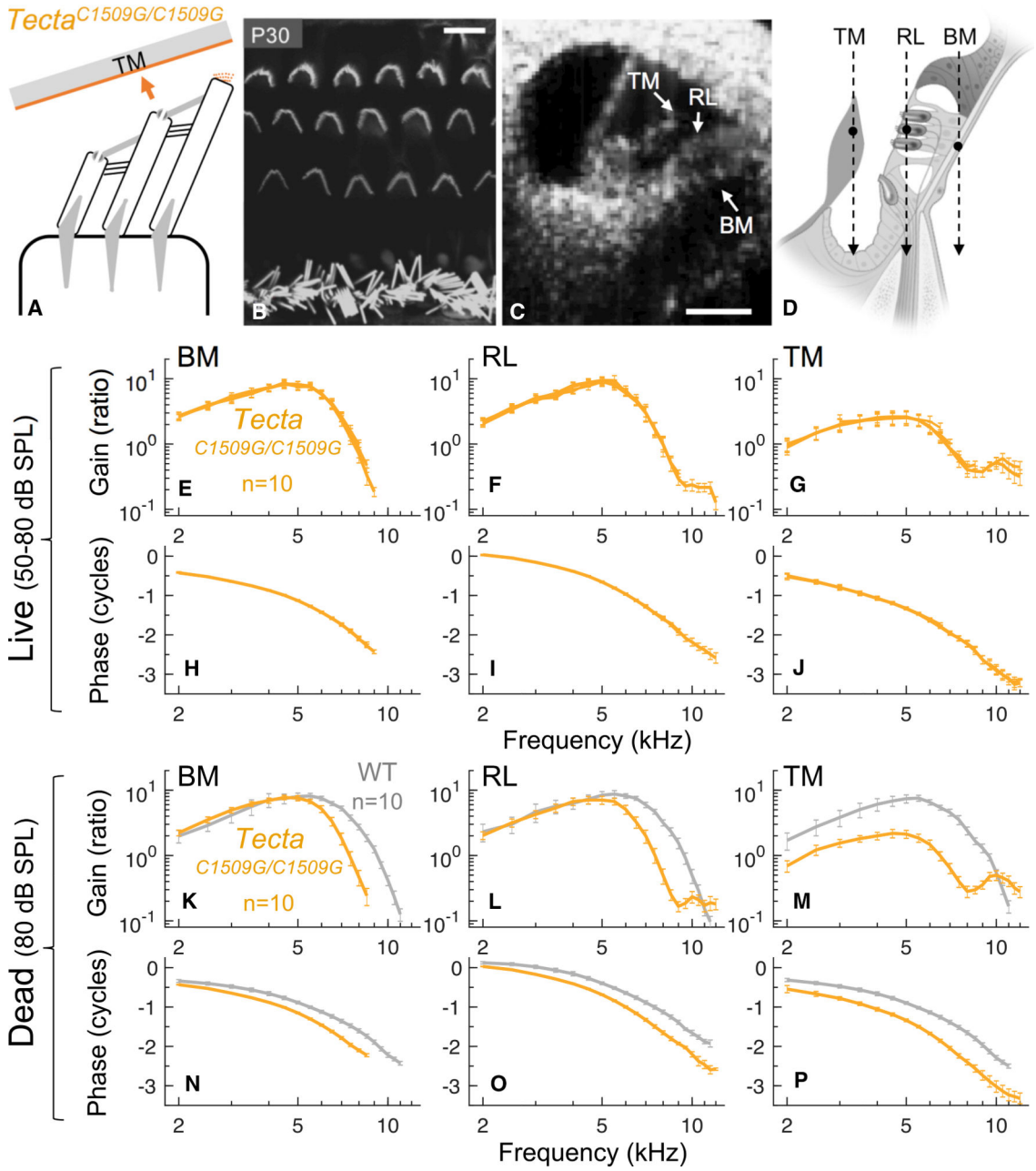

Figure 6. Vibrations in Mice with a Malformed TM and No Stereocilia-TM Attachment

(A) Cartoon illustrating that the TM does not contact the OHC stereocilia in *Tecta*$^{C1509G/C1509G}$ mice.

(B) Phalloidin-stained whole-mount image from the apical cochlear turn of a P30 *Tecta*$^{C1509G/C1509G}$ mouse demonstrating normal bundle morphology. Scale bar, 10 μm.

(C) Cross-sectional image of the apical cochlear duct from a *Tecta*$^{C1509G/C1509G}$ mouse showing that the TM is lifted away from the RL. Scale bar, 100 μm.

(D) Schematic showing the orientation of the structures used for the semi-radial vibration measurements.

(E–J) Average vibratory gains (E–G) and phases (H–J) of the BM, RL, and TM, respectively, from live *Tecta*$^{C1509G/C1509G}$ mice (n = 10), illustrating the linearity of the responses and the absence of cochlear amplification.

(K–P) Average vibratory gains (K–M) and phases (N–P) from dead *Tecta*$^{C1509G/C1509G}$ mice and dead WT CBA/CaJ mice for 80 dB SPL stimuli (n = 10 each). The high-frequency extent of the gain and phase curves was further reduced in *Tecta*$^{C1509G/C1509G}$ mice, and the gain curves peaked at lower frequencies. The TM also vibrated less in *Tecta*$^{C1509G/C1509G}$ mice than in WT.

Error bars indicate SEM.

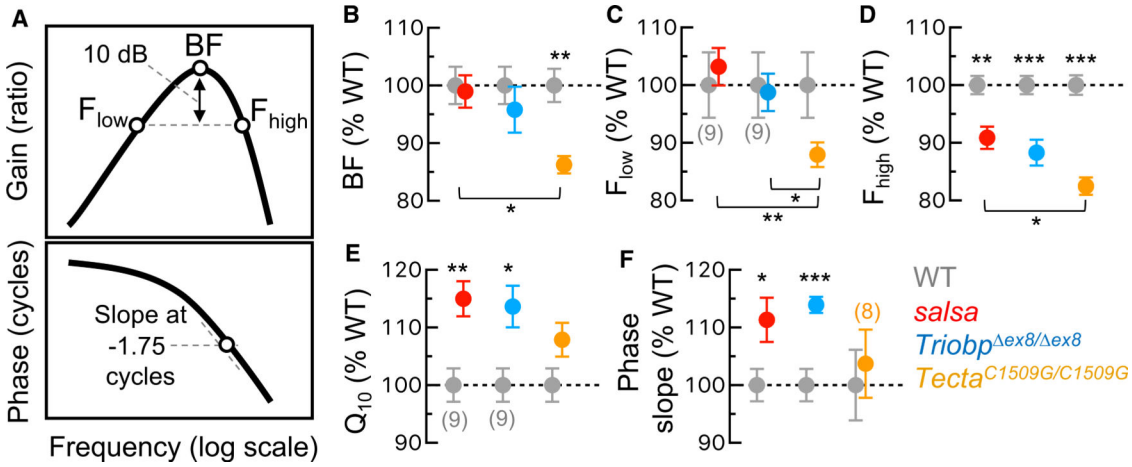

Figure 7. Quantitative Comparisons Suggest Reduced Longitudinal Coupling in *salsa* and *Triobp*$^{\Delta ex8/\Delta ex8}$ Mice and Mixed Effects in *Tecta*$^{C1509G/C1509G}$ Mice

(A) Cartoon illustrating the parameterization of individual data. Top: for each gain curve, the peak frequency (BF) and low- and high-frequency intercepts 10 dB down from the peak (F_{low} and F_{high}, respectively) were identified. Q_{10dB} was calculated as BF/(F_{high}-F_{low}). Bottom: the negative slope of the phase curve (as a function of logarithmic frequency, or octaves) was computed at the frequency where the phase crossed −1.75 cycles.

(B–F) Mean values for BF (B), F_{low} (C), F_{high} (D), Q_{10dB} (E), and phase slope (F) expressed as a percentage of the appropriate WT mean (C57BL/6J for *salsa* and *Triobp*$^{\Delta ex8/\Delta ex8}$; CBA/CaJ for *Tecta*$^{C1509G/C1509G}$). WT means (100% by definition) and SEM are shown for comparison. Means for each strain were based on data from 10 mice, unless otherwise indicated by the numbers in parentheses in (C), (E), and (F). Asterisks above each plot denote significant differences relative to WT for each mutant as assessed by unpaired *t* test. Asterisks below each plot denote significant differences between mutants as assessed by one-way ANOVA and Tukey's honestly significant difference (HSD) post hoc comparisons. *p < 0.05; **p < 0.005; ***p < 0.0005. Error bars indicate SEM.

See also Table S1.